Impact of Multi-Connectivity on Channel Capacity and Outage Probability in Wireless Networks

Lotte Weedage, Clara Stegehuis, and Suzan Bayhan

***Abstract*—Multi-connectivity facilitates higher throughput, shorter delay, and lower outage probability for a user in a wireless network. Considering these promises, a rationale policy for a network operator would be to implement multi-connectivity for all of its users. In this paper, we investigate whether the promises of multi-connectivity also hold in such a setting where all users of a network are connected through multiple links in the downlink. In particular, we consider a wireless network where every user connects to its k closest base stations. Using a framework of stochastic geometry and probability theory, we obtain analytic expressions for per-user throughput and outage probability of k-connectivity networks under several failure models. In contrast to the conclusions of previous research, our analysis shows that per-user throughput always decreases with increasing k. However, multi-connected networks are more resilient against failures than single connected networks as reflected with lower outage probability. Moreover, multi-connectivity leads to higher throughput fairness among the users. Consequently, we conclude that rather than implementing multi-connectivity for all users, a network operator should consider it for the users who would benefit from additional links the most, e.g., cell edge users.**

***Index Terms*—Capacity, multi-connectivity, outage probability, poisson point process, reliability.**

I. Introduction

MULTI-CONNECTIVITY (MC) refers to a setting in which a user is simultaneously connected to a network through multiple connections, e.g., base stations (BS). As the traffic can flow through multiple paths, a user can enjoy higher data rates, higher reliability, or lower link delays, which are essential for emerging applications such as augmented-reality requiring a high data rate or mission-critical applications such as surgery robots demanding ultra-reliable and low-latency communications (URLLC) [1]. These new services can be categorised into three groups: enhanced mobile broadband (eMBB), massive machine-type communications (mMTC) and URLLC. In addition, MC can increase the resilience of a network by exploiting spatial and frequency diversity. For instance, a user can be connected to a millimeter wave (mmWave) network which provides ample bandwidth while a second link at sub-6 GHz bands can ensure a stable connection in case the mmWave link is disrupted due to an object blocking the line-of-sight (LoS) mmWave connection. Regarding spatial diversity, a user can be connected to multiple BSs which are at different locations thereby improving communication quality, e.g., via decreasing the likelihood of correlated large-scale fading or increasing the robustness against network failures [2].

Depending on the primary goal, one of the following approaches can be used to realize MC: (i) load balancing, (ii) packet splitting, and (iii) packet duplication [3]. In *load balancing*, packets are distributed among different connections, which can increase throughput and latency in comparison to *single connectivity* (SC) networks, but does not necessarily increase reliability. Such a method would therefore be useful in eMBB, where high throughput is the main focus. Similar to load balancing, *packet splitting* distributes traffic over multiple links, but at the packet level. That is, every packet is split into multiple parts and then every part is sent over a different link. Consequently, packet splitting will reduce the latency, but will not improve reliability, which makes packet splitting suitable in mMTC applications. When the primary goal is to increase the reliability as in mission-critical applications and URLLC, *packet duplication* based MC suggests transmitting each packet over every link so that the likelihood of failure is decreased at the expense of capacity.

While the promise of MC over SC is demonstrated in the prior works such as [4], [5], a key question remains to find the optimal *degree* of MC, i.e., the number of connections per user, so that the throughput and network reliability is high. Since MC results in various complexities such as signalling overhead among multiple network nodes, traffic scheduling or combining at the receiver [2], it is desirable to find the degree of MC that achieves a significant improvement over a one-lower connectivity. To find this optimal degree, one can use different measures, such as the *spectral efficiency*, *outage probability*, and *channel capacity* of the network. In [4], the authors conclude that the optimal number of connections varies between 2 and 4 in mmWave networks based on the outage probability for cell-edge users and the spectral efficiency of the network. In this paper, we focus on eMBB and therefore will consider throughput of a randomly-selected user (not necessarily at the cell-edge) as it provides more insight on whether an application's rate requirements can be met.

Given that another motivation for MC is to increase reliability, we will also model the impact of MC on the expected channel

Manuscript received 13 April 2022; revised 18 August 2022 and 1 December 2022; accepted 30 January 2023. Date of publication 6 February 2023; date of current version 20 June 2023. This work was supported by University of Twente under the Project EERI: Energy-Efficient and Resilient Internet. The review of this article was coordinated by Prof. Hung-Yun Hsieh. *(Corresponding author: Lotte Weedage.)*

The authors are with the Faculty of Electrical Engineering, Mathematics and Computer Science, University of Twente, 7522 NB Enschede, The Netherlands (e-mail: l.weedage@utwente.nl; c.stegehuis@utwente.nl; s.bayhan@utwente.nl).

Digital Object Identifier 10.1109/TVT.2023.3242358

capacity in the face of failures as well as the outage probability which quantifies the probability that a user is disconnected from the network. These failures can be due to low SNR, the loss of LoS links as experienced in mmWave networks [4] or failures caused by wireless channel impairments. More precisely, we will address the following questions by providing an analytical framework based on stochastic geometry and probability theory:

- How does MC affect per-user throughput and outage probability of a cellular network when all links are reliable?
- How does MC affect per-user throughput and outage probability in case of various link failures?

Our analysis shows that going from SC to MC decreases per-user throughput if all users are multi-connected with equal number of connections, as resources are finite and are in this scenario divided among weaker links. Thus, while MC may increase spectral efficiency [4], the fact that BSs share their resources among more users that are possibly further away makes MC decrease per-user throughput. Hence, a key take-away of our paper is that simply increasing the number of connections of a user may not improve user throughput and MC should be leveraged for users who would benefit from it the most such as for cell edge users or users with higher rate or reliability requirements. Another observation is that higher degrees of MC increase throughput fairness among users and that MC significantly mitigates network outages under failures.

To summarize, our key contributions are twofold:

- We provide an analytical framework to analyze k-connected MC networks for arbitrary k. Different than [2] whose focus is on packet-duplication and combining schemes, we investigate MC in the form of load balancing, i.e., users are served through every connection they have without redundancy.
- We show that contrary to the single-user perspective, MC decreases per-user throughput. While some studies such as [6] point to the rate-reliability trade-off present in MC, none of these studies consider possible failures in the network. Our framework enables to analyze the outage probability for a more general class of failure models, including failures due to low SNR and loss of LoS. We quantify to what extent MC increases network reliability under several types of failure models.

In the following sections, we first overview the most relevant work in Section II. Next, we elaborate on the models for MC (Section III) and analytically find the expectation of the channel capacity of a user under MC (Section IV). Then, we investigate the outage probability under different failure models (Section V), which we can use to find the expected channel capacity after failures. We present performance analysis of the considered models in Section VI to investigate the impact of MC for wireless networks. Finally, we discuss the limitations of our work in Section VII and conclude the paper in Section VIII with some future research directions.

II. Related Work

In this section, we overview two lines of related work on MC: performance and reliability of MC and impact of failures in MC networks. We refer the reader to [3] for a broader overview of the state-of-the-art on MC.

Performance and reliability: The goal of this paper is to assess the impact of MC on network performance as well as its reliability, which was also the focus of [2], [4], [7], [8], Authors in [2] investigate the performance of MC at the packet level and provide analytical expressions for the SNR gain and outage probability in the network considering different combining approaches at the receiver for packet-duplication MC. [4] investigates the performance of MC in a mmWave urban deployment, where LoS failures are frequent. These studies provide exact expressions for the outage probability and mean spectral efficiency under LoS failures. Both papers conclude that MC improves the SNR gain and spectral efficiency over the whole network. Our work differs from [2] and [4] in several ways. First, we investigate the network from a user's perspective located anywhere in the cell and when all users are multi-connected, e.g., when for example the network operator implements a simple policy of a fixed number of connections for reliable communications. Second, our focus is on load-balancing MC as we consider eMBB applications. Finally, we model various failures and assess the impact of MC. Our conclusions show that for a single user, the average throughput will decrease under MC.

Other earlier works such as [7], [8] show that in a scenario without mobility MC always increases reliability, e.g. lower outage probability, while per-user throughput may decrease. This is sometimes referred to as the *rate-reliability trade-off* [6]. In these papers, the outage probability is defined as the probability that the SNR of a user is below a certain threshold. However, these studies use a dynamic number of links per user, which makes analytical expressions for coverage probability and throughput intractable. Therefore, these papers only provide analytical results for 1- and 2-connectivity, and present an analysis of the impact of higher degrees of connectivity via simulations. In an urban scenario, with LoS blockages of links, MC increases spectral efficiency and reliability [4]. However, often the authors only focus on a single user, and do not investigate the per-user throughput of MC, which we analyze in this work.

Impact of link failures: Little research has been done on the impact of *link failures* on the throughput and outage effects in multi-connected networks, where links can fail due to other causes than only low S(I)NR. In [4] and [9], the authors show how the loss of LoS affects the network throughput. Similarly, it has been shown that in ultra-dense urban scenarios [5], [10], [11], indoor scenarios [12] and under mobility [13], MC increases the per-user throughput. Our work differs from these papers in that we consider not only loss of LoS but a more general class of link failures, based on for example distance and channel impairments.

III. System Model

We consider the downlink of a cellular network where base stations (BS) and users (U) are distributed following a homogeneous Poisson Point Process (PPP) [14]. Although real BS locations might not always resemble a PPP [15], this is a well-known and tractable approach to modelling networks [16],

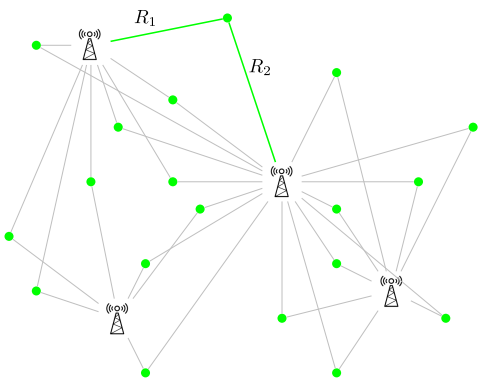

Fig. 1. Users connect to the two nearest base stations.

which can lead to important insights on real BS statistics [17], [18]. Let us denote the corresponding PPP parameters λ_{BS} and λ_U for the BSs and the users, respectively. As BS association scheme, we assume that each user in this network connects to the k BSs that are closest to the user. We refer to this MC setting as *k-connectivity*. For example, Fig. 1 depicts a 2-connectivity scenario. The network operator owns a spectrum of W_{tot} Hz and allocates this spectrum to its BSs equally using a frequency reuse factor of s, e.g., when $s = 1$, each BS operates over the whole spectrum band. We denote the bandwidth of a BS by W_{BS} and transmission power level P_{tx} Watts. We assume that a BS serves each of its users over the whole bandwidth in a time-sharing manner. Moreover, each user is reserved an equal amount of time. We denote the number of users connected to a BS by D_{BS} and refer to it as the degree of this BS. Similarly, we denote the number of connections of a user by D_U. Without failures, this means that $D_U = k$ under k-connectivity. However, when a link fails and the user is under outage, D_U can become less than k. We denote the outage probability by $\mathbb{P}(D_U = 0)$.

We denote the path loss exponent by α. Moreover, we denote the distance of a randomly-selected user to its j^{th} closest BS (BS$_j$) by R_j and the SNR from BS$_j$ by SNR$_j$. Consequently, we denote the channel capacity of the link between a user and BS$_j$ by C_j. Since we assume an MC network in which downlink traffic for each user is distributed over multiple links using *load balancing* [3], we define the channel capacity C^k_{sum} as the sum of all channel capacities that a user has from its links with BS$_j, j \in \{1, 2, \ldots, k\}$ in k-connectivity.

Let N_{BS} denote the number of BSs within a circle with radius r. Similarly, let N_U denote the number of users within a circular area with radius r. With the PPPs for the spatial distributions of BSs and users, we can calculate the probability of n BSs/users in the considered circular area as follows:

$$P(N_{BS}(\pi r^2) = n) = \frac{(\lambda_{BS}\pi r^2)^n}{n!} e^{-\lambda_{BS}\pi r^2}, \tag{1}$$

$$P(N_U(\pi r^2) = n) = \frac{(\lambda_U \pi r^2)^n}{n!} e^{-\lambda_U \pi r^2}. \tag{2}$$

Next, we derive the channel capacity of a user when it is connected to the k-closest BSs.

A. Channel Capacity Under K-Connectivity

We denote the Shannon channel capacity [19] of the link between a user and its j^{th} closest BS as C_j, $j \in \{1, 2, \ldots, k\}$. This channel capacity C_j depends on the time the BS can allocate bandwidth W_{BS} to this user, which depends on the degree of this BS, and the signal-to-noise-ratio SNR$_j$ at the considered user. Given the number of users of a BS that a given user connects to (i.e., $\tilde{D}_{BS}$) and assuming that a BS divides the time equally among its users, we can calculate C_j as follows:

$$C_j = \frac{W_{BS}}{\tilde{D}_{BS}} \log_2 (1 + \text{SNR}_j). \tag{3}$$

To find the bandwidth W_{BS} allocated to each BS, we need to know the number of BSs deployed in the coverage area (A) of the operator. Then, we derive W_{BS} as:

$$W_{BS} = \frac{W_{\text{tot}}}{s}, \tag{4}$$

where s is the frequency reuse factor. In this analytical setting, we focus on the case where $s = \lambda_{BS} \cdot A$, which means that each BS in the network is allocated exclusively its own resources and thereby experiencing no interference from the neighbouring BSs. Then,

$$W_{BS} = \frac{W_{\text{tot}}}{\lambda_{BS} A} = \frac{\overline{W_{\text{tot}}}}{\lambda_{BS}}, \tag{5}$$

where $\overline{W_{\text{tot}}} = W_{\text{tot}}/A$ is the total bandwidth per unit area. Note that this assumption facilitates analytical tractability. However, we will also investigate in Section VI via simulations the cases where frequency is reused and BS transmissions might interfere with each other in the downlink.

Assuming a transmitter operating with a transmission power P_{tx} and a receiver with a total noise power N_{tot} over the communication bandwidth, we can calculate SNR$_j$ as follows:

$$\text{SNR}_j = \frac{P_{\text{tx}} R_j^{-\alpha}}{N_{\text{tot}}(\lambda_{BS})} = \begin{cases} cR_j^{-\alpha} & R_j \geq 1, \\ c & R_j < 1. \end{cases} \tag{6}$$

With a slight abuse of notation, we define $c := c(\lambda_{BS}) = P_{\text{tx}}/N_{\text{tot}}(\lambda_{BS})$ and $N_{\text{tot}}(\lambda_{BS})$ consists of the thermal noise over the transmission band W_{BS} and the receiver's noise figure. $N_{\text{tot}}(\lambda_{BS})$ is calculated as follows [20]:

$$N_{\text{tot}}(\lambda_{BS}) = kK \frac{\overline{W_{\text{tot}}}}{\lambda_{BS}} + NF, \tag{7}$$

where $k = 1.38 \times 10^{23}$ (in Joules/Kelvin) is Boltzmann's constant, K is the temperature (in Kelvin) and NF is the noise figure of the receiver [21]. Moreover, we use the free space path loss model with path loss exponent α. Inserting (5) into (3), we obtain C_j as:

$$C_j = \frac{\overline{W_{\text{tot}}}}{\lambda_{BS} \tilde{D}_{BS}} \log_2 (1 + \text{SNR}_j). \tag{8}$$

For a load-balancing MC, we define C^k_{sum} as the sum of all channel capacities provided by all k links of this user:[1]

$$C^k_{\text{sum}} = \sum_{j=1}^{k} \frac{\overline{W_{\text{tot}}}}{\lambda_{BS}\tilde{D}_{BS}} \log_2\left(1+\text{SNR}_j\right) \text{ bits/s.} \tag{9}$$

IV. Capacity Analysis of Multi-Connectivity

In this section, we derive the expected channel capacity of a user with k connections, denoted by C^k_{sum}, assuming the system model described in Section III. Note that (9) is a product of random variables, namely $\tilde{D}_{BS}$ and SNR_j. We here assume that the degree of a BS is independent of the SNR provided by that BS to enable analytical tractability. Later in Section V we will discuss that this assumption may not hold in general. To calculate $\mathbb{E}(C^k_{\text{sum}})$ of (9), we will derive the expected degree of a BS to which a user connects, the distribution of the SNR, and finally the expectation of $\log_2(1+\text{SNR}_j)$ in the following sections.

A. Expected Degree of a Base Station

We can approximate the degree distribution of a BS by finding the area in which users connect to this BS under $k-$connectivity, which has been derived in [22]:

$$\mathbb{P}(D_{BS}=n) = \frac{\Gamma(n+a_k)}{\Gamma(n+1)\Gamma(a_k)} \frac{a_k^{a_k}(k\lambda)^n}{(k\lambda+a_k)^{a_k+n}}, \tag{10}$$

for $a_1 = 3.5, a_2 = 7.2, a_3 = 11.1, a_4 = 15.2$ and $a_5 = 21.2$ and where $\lambda = \lambda_U/\lambda_{BS}$.

However, D_{BS} is the degree distribution of a randomly chosen BS. On the other hand, $\tilde{D}_{BS}$ is the distribution of the degree of a BS which a given user connects to. As a BS with a larger number of links has more users associated with them, the average degree of a BS to which this user connects is in general higher than the average degree of a uniformly chosen BS. To be precise, $\tilde{D}_{BS}$ is given by the so-called *size-biased distribution* of D_{BS} [23, Chapter 1], which is the distribution of the degree of a BS to which a randomly chosen user connects. That is,

$$\mathbb{P}(\tilde{D}_{BS}=n) = \frac{n\mathbb{P}(D_{BS}=n)}{\mathbb{E}(D_{BS})}. \tag{11}$$

Thus, to obtain the expectation of $\overline{W_{\text{tot}}}/(\lambda_{BS}\tilde{D}_{BS})$ in (9), we can write:

$$\begin{aligned}\mathbb{E}\left(\frac{\overline{W_{\text{tot}}}}{\lambda_{BS}\tilde{D}_{BS}}\right) &= \frac{\overline{W_{\text{tot}}}}{\lambda_{BS}} \sum_{n=1}^{\infty} \frac{1}{n}\mathbb{P}\left(\tilde{D}_{BS}=n\right) \\ &= \frac{\overline{W_{\text{tot}}}}{\lambda_{BS}} \sum_{n=1}^{\infty} \frac{\mathbb{P}(D_{BS}=n)}{\mathbb{E}(D_{BS})} \\ &= \frac{\overline{W_{\text{tot}}}}{\lambda_{BS}} \frac{1}{k\lambda} = \frac{\overline{W_{\text{tot}}}}{k\lambda_U}. \end{aligned} \tag{12}$$

B. Probability Distribution of SNR

Since the SNR depends on the distance between a user and the BS in consideration, we need to find the distance distribution from a randomly chosen user to the j^{th} closest BS for all $j \in \{1,2,\ldots,k\}$. Let us denote the distance to the j^{th} closest BS by R_j (Fig. 1). We can derive the probability density of R_j by relying on the fact that the j^{th} closest BS is at a distance larger than r if and only if there are less than j BSs within the surrounding area πr^2 of this considered user. Formally, we state this probability as follows:

$$\begin{aligned}\mathbb{P}(R_j > r) &= \mathbb{P}(N_{BS}(\pi r^2) \le j-1) \\ &= \sum_{i=0}^{j-1} \frac{(\lambda_{BS}\pi r^2)^i}{\Gamma(i+1)} e^{-\lambda_{BS}\pi r^2} \\ &= \frac{\Gamma(j,\lambda_{BS}\pi r^2)}{\Gamma(j)}, \end{aligned} \tag{13}$$

where we used (1) and $\Gamma(z,x) = \int_x^\infty t^{z-1}e^{-t}\text{d}t$ is the upper incomplete gamma function. Therefore, we can write the probability density function of R_j as:

$$f_{R_j}(r) = \frac{2\left(\lambda_{BS}\pi r^2\right)^j}{r\Gamma(j)} e^{-\lambda_{BS}\pi r^2}.$$

With a slight abuse of the notation, we will refer to the SNR of the j^{th} closest BS by SNR_j. With distance distribution f_{R_j}, we can find the probability distribution of SNR_j as follows when $x < c$:

$$\mathbb{P}\left(\text{SNR}_j \le x\right) = \mathbb{P}\left(R_j \ge \left(\frac{c}{x}\right)^{\frac{1}{\alpha}}\right) = \frac{\Gamma\left(j,\phi x^{-\frac{2}{\alpha}}\right)}{\Gamma(j)},$$

where $\phi = \lambda_{BS}\pi c^{\frac{2}{\alpha}}$. Therefore,

$$f_{\text{SNR}_j}(x) = \frac{d}{dx}\left[\frac{\Gamma\left(j,\phi x^{-\frac{2}{\alpha}}\right)}{\Gamma(j)}\right] = \frac{2\left(\phi x^{-\frac{2}{\alpha}}\right)^j}{\alpha x\Gamma(j)} e^{-\phi x^{-\frac{2}{\alpha}}}.$$

Since the SNR cannot be larger than c according to (6), the probability density of the SNR becomes:

$$f_{SNR_j}(x) = \begin{cases} \frac{2\left(\phi x^{-\frac{2}{\alpha}}\right)^j}{\alpha x\Gamma(j)} e^{-\phi x^{-\frac{2}{\alpha}}}, & x < c \\ \mathbb{P}(R_j < 1) = 1 - \frac{\Gamma(j,\lambda_{BS}\pi)}{\Gamma(j)}, & x = c \\ 0 & x > c. \end{cases} \tag{14}$$

C. Expectation Logarithm of SNR_j

To find the expected channel capacity in (8), we need to find the expectation of $\log_2(1+SNR_j)$ for $j \in \{1,2,\ldots,k\}$. We define this expectation in Theorem 1 whose proof can be found in Appendix A. However, this expectation is difficult to interpret due to the presence of several special mathematical functions and their derivatives. We therefore also provide an approximation of this expectation that holds in the high SNR regime. This approximation provides more insight into the behaviour of the expected total channel capacity $\mathbb{E}(C_j)$ with respect to j.

Theorem 1: The expectation of $\log_2(1+SNR_j)$ is given in (15) shown at the bottom of the next page, where $\phi = \lambda_{BS}\pi c^{\frac{2}{\alpha}}$ and $G(j,\phi)$ is defined in (16) shown at the bottom of the next page. Moreover, for large c, $\lambda_{BS} < \frac{1}{\pi}$ and $\phi > 1$, which

[1]Note that one could account for the overhead due to load balancing by multiplying (9) with a constant $\theta < 1$.

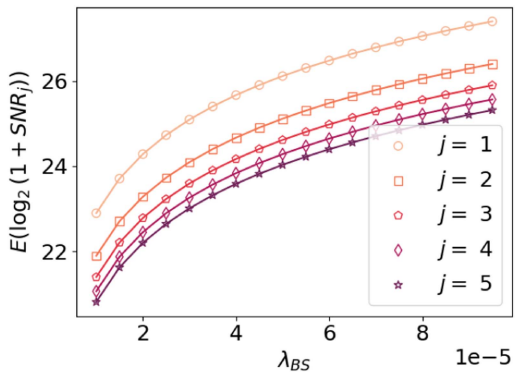

Fig. 2. Real value (line) and approximation (markers) of $\mathbb{E}(\log_2(1+\text{SNR}_j))$ for various j and with $P_{\text{tx}} = 30$ dBm and $\alpha = 2$.

corresponds to the high SNR regime, this expectation can be approximated with:

$$\mathbb{E}(\log_2(1+\text{SNR}_1)) = \frac{\alpha}{2\ln(2)}\left(\ln(\phi)+\gamma-\lambda_{BS}\pi\right)+\delta_1, \tag{17}$$

$$\mathbb{E}(\log_2(1+\text{SNR}_j)) = \frac{\alpha}{2\ln(2)}\left(\ln(\phi)+\gamma-H_{j-1}\right)+\delta_j, \tag{18}$$

for $j>1$ and where γ is Euler's constant, $H_j = \sum_{i=1}^{j}\frac{1}{i}$ is the harmonic number and for the following variables δ_1 and δ_j:

$$\delta_1 = O\left(\phi^{-1}\right)+O\left((\lambda_{BS}\pi)^2\right)+O\left(\ln(c)c^{-1}\right)+O\left(\mathbb{E}\left(\text{SNR}_1^{-1}\right)\right),$$
$$\delta_j = O\left(c^{-\frac{2j}{\alpha}}\ln(\phi)\right)+O\left(\Gamma(j)^{-1}c^{-\frac{2j}{\alpha}}\phi^{-j}\right)+O\left(\ln(c)c^{-1}\right)$$
$$+O\left(\mathbb{E}(\text{SNR}_j^{-1})\right), \qquad j>1.$$

We define the big-O notation as follows: $f(\phi) = O(g(\phi))$ as $\phi\to\infty$ if there exists a ϕ_0 and a positive real number M such that $|f(\phi)| \le Mg(\phi)$ for all $\phi > \phi_0$. To assess the accuracy of our approximation with respect to the real values calculated in (33), we show the real values and the approximation in Fig. 2. For the sake of simplicity in the calculations, we omit δ_1 and δ_j in this analysis and in the rest of the paper. Despite this, Fig. 2 shows that our approximation matches the real values with a high accuracy.

D. Expected Channel Capacity

By Theorem 1 and (12), we now have an expression for the expected channel capacity of a single user that connects to BS_j with a total of k connections per user:

$$\mathbb{E}\left(C_j^k\right) = \frac{\overline{W_{\text{tot}}}}{k\lambda_U}\cdot\mathbb{E}\left(\log_2(1+\text{SNR}_j)\right), \tag{19}$$

and its approximation, using (17) and (18):

$$\mathbb{E}\left(C_1^k\right) = \frac{\overline{W_{\text{tot}}}}{k\lambda_U}\frac{\alpha}{2\ln(2)}\left(\ln(\phi)+\gamma-\lambda_{BS}\pi\right)+\delta_1, \tag{20}$$

$$\mathbb{E}\left(C_j^k\right) = \frac{\overline{W_{\text{tot}}}}{k\lambda_U}\frac{\alpha}{2\ln(2)}\left(\ln(\phi)+\gamma-H_{j-1}\right)+\delta_j, j>1. \tag{21}$$

Note that we assume that the expected degree of a BS and the distance to this BS are independent. While this assumption is realistic for larger values of k where the degree distribution becomes more concentrated [22], it may not always hold as we will show in Section V. For $k>1$, we are interested in the sum of the channel capacities, C_{sum}^k, as defined in (9):

$$\begin{aligned}\mathbb{E}(C_{\text{sum}}^k) &= \sum_{j=1}^{k}\mathbb{E}(C_j^k)\\ &= \frac{\overline{W_{\text{tot}}}}{k\lambda_U}\frac{\alpha}{2\ln(2)}\left(k\ln(\phi)+k\gamma-\lambda_{BS}\pi-\sum_{j=1}^{k-1}H_j\right)\\ &= \frac{\overline{W_{\text{tot}}}}{k\lambda_U}\frac{\alpha}{2\ln(2)}\left(k\ln(\phi)+k\gamma-\lambda_{BS}\pi-kH_k+k\right)\\ &= \frac{\overline{W_{\text{tot}}}}{\lambda_U}\frac{\alpha}{2\ln(2)}\left(\ln(\phi)+\gamma+1-\left(H_k+\frac{\lambda_{BS}\pi}{k}\right)\right),\end{aligned} \tag{22}$$

where we used the property of harmonic numbers: $\sum_{j=1}^{k-1}H_j = kH_k - k$.

Theorem 2: In the high SNR regime, the sum of the channel capacities, $\mathbb{E}(C_{\text{sum}}^k)$, as defined in (22), is decreasing in k.

Proof: As a large part of (22) does not depend on k, we only need to focus on the part $H_k+\frac{\lambda_{BS}\pi}{k}$. Assume $k\ge 1, k\in\mathbb{N}$. Then, for $k+1$:

$$H_{k+1}+\frac{\lambda_{BS}\pi}{k+1} = H_k+\frac{1+\lambda_{BS}\pi}{k+1} > H_k+\frac{\lambda_{BS}\pi}{k},$$

$$\mathbb{E}(\log_2(1+SNR_j)) = \frac{1}{\ln(2)\Gamma(j)}G(j,\phi)+\log_2(1+c)\left(1-\frac{\Gamma(j,\lambda_{BS}\pi)}{\Gamma(j)}\right)$$
$$+\frac{\alpha}{2\ln(2)\Gamma(j)}\left(\ln(\phi)\left(\Gamma(j,\lambda_{BS}\pi)-\Gamma(j,\phi)\right)-\frac{\mathrm{d}}{\mathrm{d}a}\left[\Gamma(a,\lambda_{BS}\pi)-\Gamma(a,\phi)\right]_{a=j}\right) \tag{15}$$

$$G(j,\phi) = \sum_{i=0}^{\infty}\frac{(-1)^i\phi^{\frac{\alpha}{2}(i+1)}}{i+1}\Gamma\left(\frac{-\alpha}{2}(i+1)+j,\phi\right)+\frac{(-1)^i\phi^{-\frac{\alpha}{2}(i+1)}}{i+1}\left(\Gamma\left(\frac{\alpha}{2}(1+i)+j,\lambda_{BS}\pi\right)-\Gamma\left(\frac{\alpha}{2}(1+i)+j,\phi\right)\right) \tag{16}$$

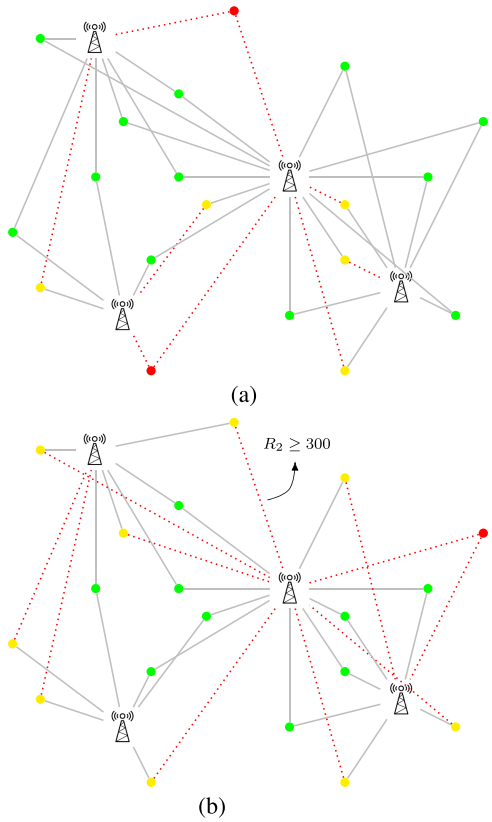

Fig. 3. Different failure models, where the red dotted, thick links have failed. Green users are still connected; yellow users are partially connected; and red users are disconnected from the network. (a) Random failure $p = 0.25$. (b) Distance failure, $r_{max} = 300$ m.

which holds for $\lambda_{BS}\pi < 1$. Thus, for $k+1$, we subtract by a larger value in (22), and hence $\mathbb{E}(C^k_{\text{sum}})$ decreases in k. ■

We use $\mathbb{E}(C^k_{\text{sum}})$ as a measure to compare different degrees of MC under various failures in the following section.

V. Impact of Link Failures on Multi-Connectivity Capacity and Outage Probability

We now investigate the performance of MC networks under the following failure models, some of which are illustrated in Fig. 3:

1) *Random failures:* In this case, each link fails with a probability p. This scenario might reflect connection failures because of wireless channel impairments due to heavy rainfall in mmWave networks. These failures can easily be extended to random BS failures, which reflect random software or hardware failures at a BS.
2) *Distance failures:* In this case, a link fails when the distance between the user and the BS is higher than a certain threshold. This failure reflects the cases where the link SNR is not high enough to ensure successful decoding of the signal. Hence, if the SNR is lower than a threshold value, the link will fail.
3) *LoS failures:* In this case, a link fails because of a lack of LoS with the user. This scenario reflects the case of mmWave links in 5G networks.

We consider the sum of the channel capacities of a user that is connected to $\text{BS}_j, j \in \{1, 2, \ldots, k\}$, where BS_1 is the closest and BS_k is the furthest one. The expected channel capacity under failures can be written as:

$$\mathbb{E}\left(C^k_{\text{sum}}\right) = \sum_{j=1}^{k} \mathbb{E}\left((1-p_j)C^k_j\right), \tag{23}$$

where p_j is the probability that the link to BS_j fails and C_j is defined in (8). Below, we derive analytic expressions for p_j for the above-listed failure models. The second quantity we investigate is the outage probability, $\mathbb{P}(D_U = 0)$, defined as the probability that a user has no connections.

In our analysis, we will consider two cases: *with instantaneous reallocation* and *without reallocation* of resources after a link failure. In the case of instantaneous reallocation, we assume that a BS re-allocates the time reserved for the failed link(s) among its currently-active links. This means that in the expected channel capacity (9), we divide by the degree of the BS after failures, which leads to an increase in service time of each connected user. Meanwhile, without reallocation, time allocated to each user remains the same (resulting in waste of available service time). These two cases can be seen as a lower and upper bound on the channel capacity after failures: in realistic scenarios the packets will be delivered after failures via the remaining links using for example coordinated multipoint (CoMP) [24] or fast switching [25].

In the following, we find exact expressions for the expected channel capacity and the outage probability without reallocation and without interference. After that, we provide numerical results on failures with and without reallocation and considering interference.

A. Random Failures

Under random failures, every BS-U link fails with probability p. Therefore, (23) becomes:

$$\mathbb{E}\left(C^k_{\text{sum}}\right) = \frac{\overline{W_{\text{tot}}}}{k\lambda_U}(1-p)\sum_{j=1}^{k}\mathbb{E}\left(\log_2\left(1+\text{SNR}_j\right)\right), \tag{24}$$

where we obtain $\mathbb{E}(\log_2(1+\text{SNR}_j))$ from Theorem 1.

The outage probability under random failures is:

$$\mathbb{P}(D_U = 0) = \mathbb{P}(\text{every link fails}) = p^k. \tag{25}$$

B. Distance Failures

In this case, a link fails deterministically when the distance between the user and its associated BS is larger than r_{max}. This distance r_{max} can be interpreted as the maximum distance such that the SNR is above a certain threshold. Then, the probability that link j fails can be derived from (13) as follows:

$$p_j = \mathbb{P}\left(R_j > r_{\text{max}}\right) = \frac{\Gamma\left(j, \lambda_{BS}\pi r^2_{\text{max}}\right)}{\Gamma(j)}, \tag{26}$$

Consequently, $\mathbb{E}(C^k_{\text{sum}})$ can be defined as follows:

$$\begin{aligned}\mathbb{E}\left(C^k_{\text{sum}}\right) &= \frac{\overline{W_{\text{tot}}}}{k\lambda_U}\sum_{j=1}^{k}(1-p_j)\mathbb{E}\left(\log_2(1+\text{SNR}_j)|R_j \le r_{\max}\right)\\ &= \frac{\overline{W_{\text{tot}}}}{k\lambda_U}\sum_{j=1}^{k}\mathbb{P}(R_j \le r_{\max})\frac{\mathbb{E}(\log(1+\text{SNR}_j), R_j \le r_{\max})}{\mathbb{P}(R_j \le r_{\max})}\\ &= \frac{\overline{W_{\text{tot}}}}{k\lambda_U}\sum_{j=1}^{k}\left(\int_1^{r_{\max}}\log_2(1+cr^{-\alpha})f_{R_j}(r)\text{d}r\right.\\ &\quad\left.+\log_2(1+c)\left(1-\frac{\Gamma(j,\lambda_{BS}\pi)}{\Gamma(j)}\right)\right),\end{aligned} \tag{27}$$

where the last term comes from the case $R_j \le 1$ in the definition of the SNR in (6), in which case the SNR equals c.

For the outage probability, we calculate the probability that the first link (hence from the closest BS) of a user fails. Since all other links are established with more distant BSs, they will also fail when the first link fails. Therefore, we calculate the outage probability as follows:

$$\mathbb{P}(D_U = 0) = \mathbb{P}(R_1 \ge r_{\max}) = e^{-\lambda_{BS}\pi r^2_{\max}}. \tag{28}$$

C. LoS Failures

We now investigate LoS failures, where a link between a user and a BS fails if the link is non-LoS. Different from the distance failures, these LoS failures happen with a certain probability based on distance instead of deterministically when the distance is above a certain threshold $r_{\max}$. There are several LoS models, e.g., based on a Poisson-distributed blockers [9], a real-life indoor scenario [26] or blockage effects by humans and buildings in an urban network [4]. We use the non-LoS probability as given in [4], [27]:

$$p_j = \begin{cases}0, & R_j \le r_{\text{LoS}},\\ 1 - R_j^{-1}\left(r_{\text{LoS}} + R_j e^{\frac{-R_j}{2r_{\text{LoS}}}} - 18e^{\frac{-R_j}{2r_{\text{LoS}}}}\right), & R_j > r_{\text{LoS}},\end{cases}$$

where r_{LoS} is a parameter that describes at what distance objects are more likely to become non-LoS. We define:

$$g(r) = r^{-1}\left(r_{\text{LoS}} + re^{\frac{-r}{2r_{\text{LoS}}}} - 18e^{\frac{-r}{2r_{\text{LoS}}}}\right). \tag{29}$$

Then, the expected channel capacity under LoS failures equals:

$$\begin{aligned}\mathbb{E}(C^k_{\text{sum}}) &= \frac{\overline{W_{\text{tot}}}}{k\lambda_U}\sum_{j=1}^{k}\mathbb{E}\left((1-p_j)\log_2(1+\text{SNR}_j)\right)\\ &= \frac{\overline{W_{\text{tot}}}}{k\lambda_U}\sum_{j=1}^{k}\mathbb{E}\left(\log_2(1+\text{SNR}_j^{-\alpha}, R_j \le r_{\text{LoS}}\right)\\ &\quad+\mathbb{E}\left((1-p_j)\log_2(1+\text{SNR}_j^{-\alpha}, R_j > r_{\text{LoS}}\right)\right)\\ &= \frac{\overline{W_{\text{tot}}}}{k\lambda_U}\sum_{j=1}^{k}\left(\mathbb{E}\left(\log_2(1+\text{SNR}_j), R_j \le r_{\text{LoS}}\right)\right.\\ &\quad\left.+\int_{r_{\text{LoS}}}^{\infty}g(r)\log_2(1+cr^{-\alpha})f_{R_j}(r)\text{d}r\right).\end{aligned} \tag{30}$$

TABLE I
SIMULATION PARAMETERS

Parameter	Value
λ_{BS}	5 BS/km^2
λ_U	500 users/km^2
α	2
P_{tx}	30 dBm
NF	5 dB [28]
W_{tot}	100 MHz
area	1km $\times$ 1km

Under the assumption that links fail independently, the outage probability becomes:

$$\begin{aligned}\mathbb{P}(D_U = 0) &= \prod_{j=1}^{k}\mathbb{P}(\text{link } i \text{ fails}) = \prod_{j=1}^{k}\mathbb{E}(p_j)\\ &= \prod_{j=1}^{k}\int_{r_{\text{LoS}}}^{\infty}(1-g(r))f_{R_j}(r)\text{d}r\\ &= \prod_{j=1}^{k}\left(\mathbb{P}(R_j \ge r_{\text{LoS}}) - \int_{r_{\text{LoS}}}^{\infty}g(r)f_{R_j}(r)\text{d}r\right)\\ &= \prod_{j=1}^{k}\frac{\Gamma(j, r^2_{\text{LoS}}\lambda_{BS}\pi)}{\Gamma(j)} - \int_{r_{\text{LoS}}}^{\infty}g(r)f_{R_j}(r)\text{d}r.\end{aligned} \tag{31}$$

VI. Performance Analysis

In this section, we provide a performance analysis of MC using system level Monte-Carlo simulations. Unless stated otherwise, we use the parameters given in Table I. We simulate each scenario 1000 times and report the averages of all runs along with 95% confidence intervals. To avoid border-effects (e.g., BS at the borders have less connected users), we assume a torus where borders are connected.

First, in Section VI-A, we evaluate the accuracy of our analytical model by comparing the results obtained from the simulations with the analytical results from Section V, leaving out δ_1 and δ_j in (20) and (21). Afterwards, we analyse a more realistic scenario by taking interference into account in Section VI-B. The analysis is based on two performance metrics: the average channel capacity (C^k_{sum}) and the outage probability under failures. Moreover, we investigate how *resilient* the network is with respect to the failures by calculating the throughput with or without reallocation.

In these simulations, we calculated the average channel capacity using the signal-to-interference-plus-noise-ratio (SINR) assuming a frequency reuse factor $s = 1$, which means that every BS operates on the same frequency. Then, we define SINR as follows:

$$\text{SINR}_j = \frac{P_{\text{tx}}R_j^{-\alpha}}{N_{\text{tot}}(\lambda_{BS}) + P_{\text{tx}}\sum_{i\in\{\text{BS}^-\}}R_i^{-\alpha}}, \tag{32}$$

where BS^- is the set of BSs that interfere with the BS in consideration, taking into account the frequency reuse factor. In the case of $s = 1$, this is the set of all BSs.

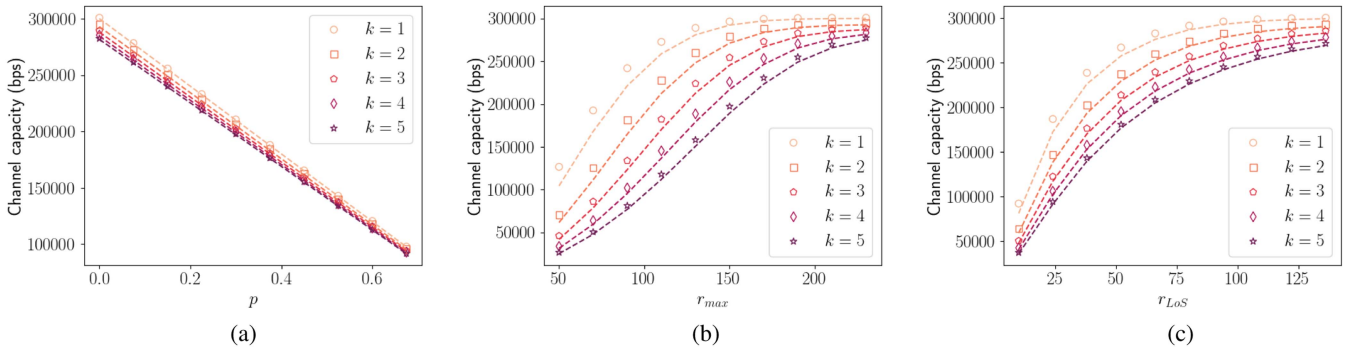

Fig. 4. Impact of parameters $p, r_{\max}$ and r_{LoS} on simulated (markers) and calculated (line) channel capacity. (a) $\mathbb{E}\left(C^k_{\text{sum}}\right)$- random failure. (b) $\mathbb{E}\left(C^k_{\text{sum}}\right)$- distance failure. (c) $\mathbb{E}\left(C^k_{\text{sum}}\right)$- LoS failure.

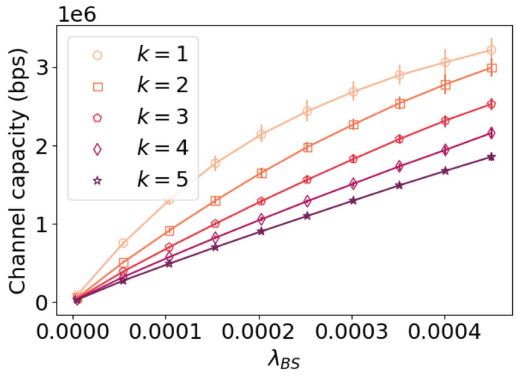

Fig. 5. Impact of increasing BS density on the channel capacity for various k-connectivity settings (simulations).

A. Accuracy of the Analytical Model

Fig. 4 depicts the change in channel capacity (without interference) under all failure models. In this figure, dotted lines represent the analytical expressions of the channel capacities from (24) for random failures, (27) for distance failures, and (30) for LoS failures. Since we only have an analytical expression in the high-SNR regime, we show these simulations for $\lambda_{BS} = 5 \cdot 10^{-5}$. While matching the trend for all failure models, the analytical values deviate from the results obtained from the simulations. We attribute this deviation to the assumption that the degree of a BS (D_{BS}) and the distance to that BS (R_j) are independent. This assumption may not hold in general as low-degree BSs most likely only serve a small area. Therefore, the distance from a user to that BS is also small resulting in higher throughput for these users as a result of higher SNR. Hence, we observe in the figures higher capacity obtained from simulations. However, for $k \geq 2$, this dependence becomes less prominent as the areas that BSs serve become larger and more equally distributed [22]. As a result, we observe a marginal gap between the results of our analytical model and the simulations.

B. Realistic Deployment

Fig. 5 shows the channel capacity with increasing BS densities for various degrees of MC without failures. We observe that for all BS deployment densities, MC decreases the channel capacity, i.e., single connectivity $k = 1$ achieves the highest capacity. For example, for $\lambda_{BS} = 5 \cdot 10^{-5}$, this decrease in comparison to SC is 32.6% for dual connectivity and 63.5% for 5-connectivity. This observation confirms the validity of Theorem 2 which shows that MC decreases the channel capacity.

Now, let us analyze the impact of link failures. Figs. 6–8 depict the channel capacity and outage probability under different failures with and without reallocation. We will first focus on the case where the BSs do not reallocate the bandwidth of the failing links. From Figs. 6(a), 7(a) and 8(a), we can see that increasing failure probability (e.g., higher p or lower $r_{\max}$ and r_{LoS}) decreases the capacity of all k-connectivity schemes. In comparison to $k = 1$, there is a maximum relative loss of respectively 39.1%, 56.8% and 47.9% for random, distance and LoS failures under dual connectivity. However, we observe that the decrease is faster for lower k values (e.g., represented as a higher slope). Despite this faster decrease, the achieved capacity is still higher compared to that of higher k. While MC schemes achieve lower outage as seen in Figs. 6(c) and 8(c), even if a user has more links that might survive after a failure, these links are with further away BSs. This results in lower throughput as the SNR from more distant BSs is lower compared to the user's first link with the closest BS. Also, with increasing MC, time allocated to each user decreases, which results in lower per-user capacity (Theorem 2).

Now, let us discuss how resource reallocation affects the capacity for different failure models and degrees of MC. Comparing Fig. 6(a) and (b), we observe that resource reallocation helps maintaining the same capacity despite the existence of failures. Since failures are random and each user-BS link is equally likely to fail independent of the distance between the user and BS, on the average, the capacity remains unchanged as active links in a BS get the time allocated to the failing links. On the other hand, we observe a different trend in Fig. 7(a) and (b) as well as in Fig. 8(a) and (b). Here, when the resources are not reallocated, with increasing $r_{\max}$ and r_{LoS}, channel capacity increases. In contrast, when reallocation is possible, the channel capacity decreases. However, note that reallocation always yields higher or equal throughput than that of without reallocation (note the difference in scale in the y-axis). Since links that are further away

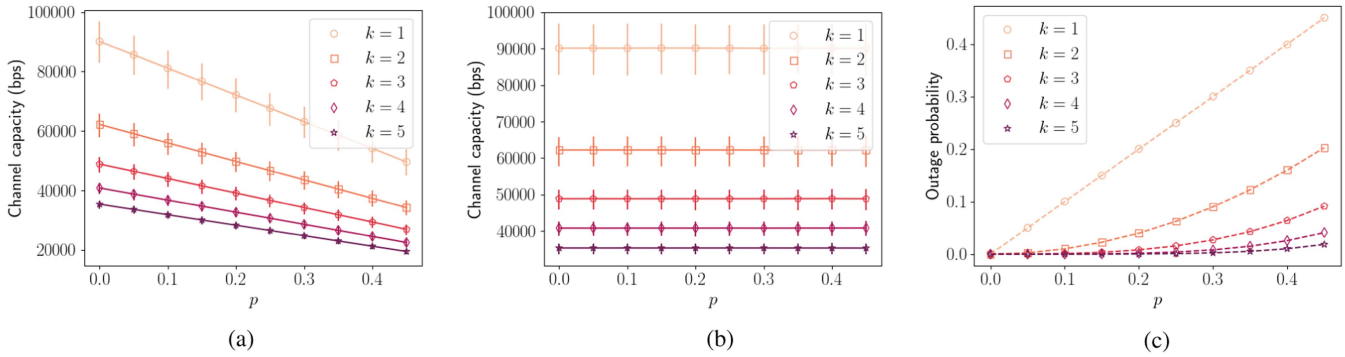

Fig. 6. Random failures. Impact of outage probability p on simulated channel capacity and outage probability. (a) $\mathbb{E}\left(C_{\text{sum}}^{k}\right)$- without reallocation. (b) $\mathbb{E}\left(C_{\text{sum}}^{k}\right)$- with reallocation. (c) Outage probability. The dotted lines showthe analytical value as given in (25).

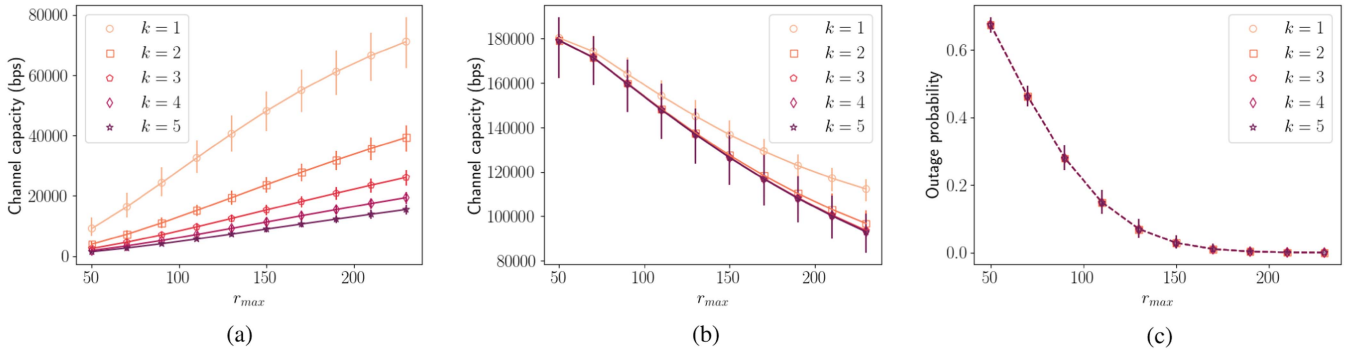

Fig. 7. Distance failures. Impact of parameter r_{max} on simulated channel capacity and outage probability. (a) $\mathbb{E}\left(C_{\text{sum}}^{k}\right)$- without reallocation. (b) $\mathbb{E}\left(C_{\text{sum}}^{k}\right)$- with reallocation. (c) Outage probability. The dotted lines show the analytical value as given in (28).

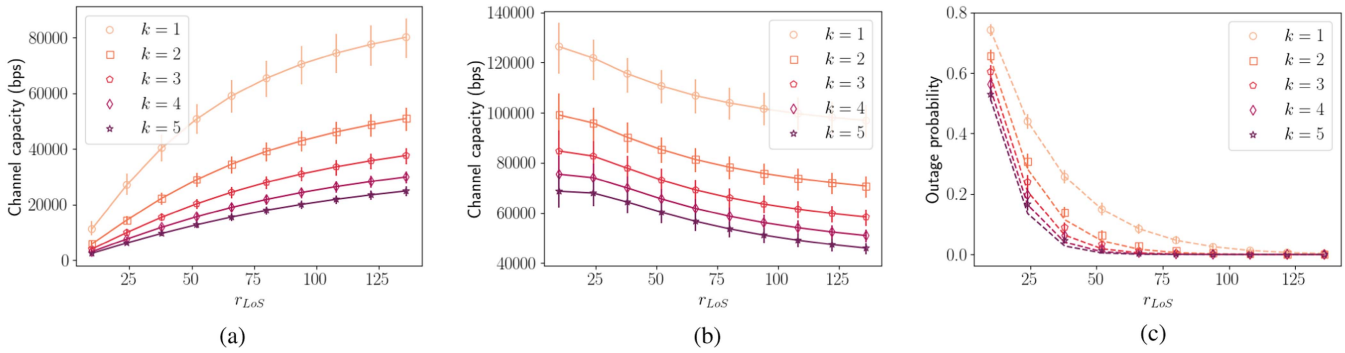

Fig. 8. LoS failures. Impact of parameter r_{LoS} on simulated channel capacity and outage probability. (a) $\mathbb{E}\left(C_{\text{sum}}^{k}\right)$- without reallocation. (b) $\mathbb{E}\left(C_{\text{sum}}^{k}\right)$- with reallocation. (c) Outage probability. The lines show the analytical value as given in (31).

will break down under distance or LoS failures, this means that the resources that get re-allocated will be assigned to links that are closer and thus will result in higher channel capacity.

As observed in the prior work such as [6], MC presents us with a rate-reliability trade-off: our simulations show a lower capacity for higher MC, but also a higher reliability as observed in Fig. 6(c) and Fig. 8(c). However, as we see in Fig. 7(c), MC does not bring any benefits for distance related failures as the failure of the first link implies failure of the additional links. Considering the improvement in outage probability under random failures, the highest improvement from k to $k+1$ connectivity is achieved for dual connectivity. This outage probability decrease enabled by a second link is especially visible for random failures for $p \sim 0.1$ in Fig. 6(c) and $r_{\text{LoS}} \sim 40$ in Fig. 8(c). While higher k decreases the outage probability further, the gain diminishes. Hence, one can argue that if the link failure probability is expected to be low, dual connectivity can facilitate the highest gains without resulting in a significant capacity loss or overhead to maintain multiple links (e.g., scheduling coordination among the BSs). Moreover, it is worth mentioning that we observe

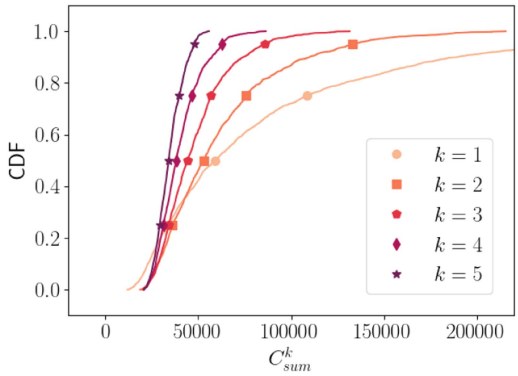

Fig. 9. Cumulative distribution of C^k_{sum}.

almost a perfect match between the analytical and simulated values of outage probability in Figs. 6(c) and 7(c).

Lastly, Fig. 9 shows that the distribution of C^k_{sum} over all users and we can see that capacity becomes more concentrated around the mean for larger values of k, as the coefficient of variation decreases. Thus, the average performance degrades, but *fairness* increases implying that users maintain similar throughput. To illustrate this, we calculated Jain's fairness index [29] of the channel capacity. This fairness index increases for higher degrees of MC: as for $k = 1$, the fairness is 0.53 and it is 0.96 for $k = 5$. Furthermore, for a given C^k_{sum}, more users maintain a given rate in higher MC in comparison to single connectivity. Thus, MC degrades the average channel capacity, but increases the channel capacity for the poorly-connected users (e.g., with lower capacity at the cell-edge).

VII. Discussion

Our analysis relies on two key assumptions. First, BSs and users are homogeneously distributed according to a Poisson point process. Second, in the analytical model, the BSs are allocated separate channels hence the interference from the adjacent cells is zero. While the first assumption is necessary for analytical tractability and it is a typical assumption in the literature, a more realistic analytical model considering heterogeneous PPP or hexagonal grids can represent the current network deployments better. Similarly, simulations can use real BS location information to account for the heterogeneity of the BS distribution in a cellular network. Regarding the second assumption, this assumption holds under appropriate frequency planning, e.g., with larger frequency reuse factor. An interesting direction is to explore whether the observed trends are also valid in the existence of co-channel interference.

We also assumed that the degree of a BS is independent of the distance between a user and a BS. However, as Fig. 5 shows, this may not hold. For further research, one could look into the dependency between these two quantities to find more accurate analytical expressions. However, for larger values of k, this error becomes significantly smaller, showing that this assumption is reasonable for MC.

We believe that there may be other policies that can make MC beneficial to the user, also in terms of an increased channel capacity. For example a heterogeneous association scheme for MC in which other properties of a user are also considered in MC decision. For instance, cell-edge users can have more connections to prevent outage for these users and to ensure higher throughput. Similarly, more sophisticated BS association schemes, e.g., BS load-aware, can be considered rather than the simple policy of connecting to the k closest BSs. Or, we could take into account beamforming for mmWave [30] or intelligent reflecting surfaces [31], [32] to increase the channel gains and therefore changing the optimal user association scheme. Designing policies ensuring that MC is exploited in such a way that all users benefit from it is therefore an important topic for further research.

VIII. Conclusion

In this paper, we have investigated the performance of a cellular network with increasing degree of multi-connectivity (MC) in terms of per-user throughput and outage probability, using a model based on stochastic geometry. Interestingly, we observed that per-user throughput decreases for higher degrees of MC, i.e., when every user connects to multiple BSs. This is in contrast with some previous results for the spectral efficiency [2], [4], which increased for moderate levels of MC. This shows that it is important to take the multi-user perspective into account when designing more efficient methods of realising MC. While our simulations and analytical model showed that MC decreases the average channel capacity, we also observed that some users still experience a higher channel capacity under MC compared to single connectivity. Additionally, MC yields a more fair distribution of the throughput in the network. Our analysis reveals the benefit of MC as increased reliability of the network under random and LoS failures. However, when failure probability increases with increasing distance between the user and the BS, then MC does not offer any increase in reliability. Since our analysis shows that simply realising MC for every user in the network does not improve throughput, network operators should design more sophisticated MC schemes e.g., considering different rate requirements and SNR of the users or use a *dynamic* number of connections per user, that can lead to performance improvements. Hence, future research directions include investigation of different association schemes as well as different MC implementations such as packet duplication for higher reliability.

Appendix A
Proof of Theorem 1

Proof: We want to find the expectation of the logarithm of SNR_j for $j \in \{1, 2, \ldots, k\}$, which is the following integral:

$$\mathbb{E}\left(\log_2\left(1 + \text{SNR}_j\right)\right) = \frac{1}{\ln(2)} \int_0^\infty \ln(1+x) f_{SNR_j}(x) \mathrm{d}x$$

We split this integral in two ranges to be able to approximate the logarithm in this integral with a Taylor expansion, which has a different form for $x \leq 1$ and $x > 1$:

$$\mathbb{E}\left(\log_2\left(1 + \text{SNR}_j\right)\right) = \frac{1}{\ln(2)} \left(I_1 + I_2 + I_3\right) + R, \qquad (33)$$

where $R = \log_2(1+c)\left(1 - \frac{\Gamma(k,\lambda_{BS}\pi)}{\Gamma(k+1)}\right)$, the point mass in $x = c$, $f_{SNR_j}(x)$ is given in (14) and I_1, I_2 and I_3 are defined as:

$$I_1 = \int_0^1 \ln(1+x) f_{\text{SNR}_j}(x)\mathrm{d}x, \tag{34}$$

$$I_2 = \int_1^c \ln\left(1+\frac{1}{x}\right) f_{\text{SNR}_j}(x)\mathrm{d}x, \tag{35}$$

$$I_3 = \int_1^c \ln(x) f_{\text{SNR}_j}(x)\mathrm{d}x. \tag{36}$$

To simplify notation, we define $\phi = \lambda_{BS}\pi c^{\frac{2}{\alpha}}$. To find an expression for I_1 and I_2, we use a Taylor expansion for the logarithm:

$$\ln(1+x) = \begin{cases} \sum_{i=0}^{\infty} \frac{(-1)^i}{i+1} x^{i+1}, & 0 \le x \le 1, \\ \ln(x) + \sum_{i=0}^{\infty} \frac{(-1)^i}{i+1} x^{-(i+1)}, & x > 1. \end{cases}$$

Therefore,

$$\begin{aligned} I_1 &= \frac{2\phi^j}{\alpha\Gamma(j)} \int_0^1 \ln(1+x) x^{-\frac{2j}{\alpha}-1} e^{-\phi x^{-\frac{2}{\alpha}}}\mathrm{d}x \\ &= \frac{2\phi^j}{\alpha\Gamma(j)} \sum_{i=0}^{\infty} \frac{(-1)^i}{i+1} \int_0^1 x^{-\frac{2j}{\alpha}+i} e^{-\phi x^{-\frac{2}{\alpha}}}\mathrm{d}x. \end{aligned} \tag{37}$$

We use the change of variables $y = \phi x^{-\frac{2}{\alpha}}$:

$$\begin{aligned} I_1 &= \frac{1}{\Gamma(j)} \sum_{i=0}^{\infty} \frac{(-1)^i \phi^{\frac{\alpha}{2}(i+1)}}{i+1} \int_{\phi}^{\infty} y^{-\frac{\alpha}{2}(i+1)+j-1} e^{-y}\mathrm{d}y \\ &= \frac{1}{\Gamma(j)} \sum_{i=0}^{\infty} \frac{(-1)^i \phi^{\frac{\alpha}{2}(i+1)}}{i+1} \Gamma\left(-\frac{\alpha}{2}(i+1)+j, \phi\right). \end{aligned} \tag{38}$$

For I_2, we use the same approach:

$$\begin{aligned} I_2 &= \frac{2\phi^j}{\alpha\Gamma(j)} \int_1^c \ln\left(1+\frac{1}{x}\right) x^{-\frac{2}{\alpha}-1} e^{-\phi x^{-\frac{2}{\alpha}}}\mathrm{d}x \\ &= \frac{2\phi^j}{\alpha\Gamma(j)} \sum_{i=0}^{\infty} \frac{(-1)^i}{i+1} \int_1^c x^{-\frac{2}{\alpha}-i-2} e^{-\phi x^{-\frac{2}{\alpha}}}\mathrm{d}x \\ &= \frac{1}{\Gamma(j)} \sum_{i=0}^{\infty} \frac{(-1)^i \phi^{-\frac{\alpha}{2}(i+1)}}{i+1} \int_{\lambda_{BS}\pi}^{\phi} y^{\frac{\alpha}{2}(i+1)+j-1} e^{-y}\mathrm{d}y \\ &= \frac{1}{\Gamma(j)} \sum_{i=0}^{\infty} \frac{(-1)^i \phi^{-\frac{\alpha}{2}(i+1)}}{i+1} \\ &\left(\Gamma\left(\frac{\alpha}{2}(1+i)+j, \lambda_{BS}\pi\right) - \Gamma\left(\frac{\alpha}{2}(1+i)+j, \phi\right)\right), \end{aligned} \tag{39}$$

with the same change of variables as we used for I_1.

For I_3 we use a slightly different approach:

$$\begin{aligned} I_3 &= \frac{2\phi^j}{\alpha\Gamma(j)} \int_1^c \ln(x) x^{-\frac{2j}{\alpha}-1} e^{-\phi x^{-\frac{2}{\alpha}}}\mathrm{d}x \\ &= \frac{\alpha}{2\Gamma(j)} \int_{\lambda_{BS}\pi}^{\phi} \ln\left(\frac{\phi}{y}\right) y^{j-1} e^{-y}\mathrm{d}y \\ &= \frac{\alpha}{2\Gamma(j)} \int_{\lambda_{BS}\pi}^{\phi} (\ln(\phi) - \ln(y)) y^{j-1} e^{-y}\mathrm{d}y \\ &= \frac{\alpha}{2\Gamma(j)} \left(\ln(\phi)\left(\Gamma(j,\lambda_{BS}\pi) - \Gamma(j,\phi)\right) \right. \\ &\left. - \int_{\lambda_{BS}\pi}^{\phi} \ln(y) y^{j-1} e^{-y}\mathrm{d}y \right) \\ &= \frac{\alpha}{2\Gamma(j)} \left(\ln(\phi)\left(\Gamma(j,\lambda_{BS}\pi) - \Gamma(j,\phi)\right) \right. \\ &\left. - \frac{\mathrm{d}}{\mathrm{d}a}\left[\Gamma(a,\phi) - \Gamma(a,\lambda_{BS}\pi)\right]_{a=j} \right), \end{aligned} \tag{40}$$

with the same changes of variables as in I_1 and I_2 and we can derive the last equation since this integrand is the derivative of the incomplete gamma function.

In (41), shown at the bottom of the next page, we filled in (33) with (38), (39) and (40), with $G(j,\phi)$ as defined in (42), shown at the bottom of the next page, which gives the result we wanted to prove. ■

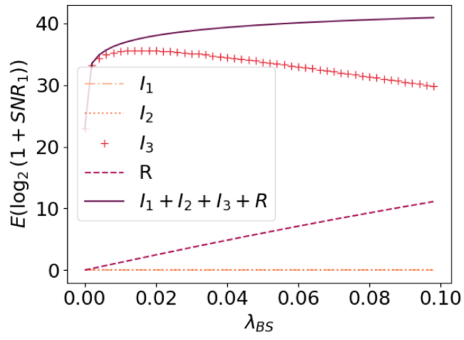

(a)

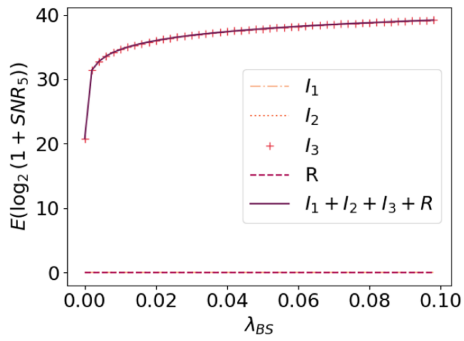

(b)

Fig. 10. $\mathbb{E}(\log_2(1+\text{SNR}_j))$ for different values of j, as a sum of I_1, I_2, I_3 and R. (a) $j = 1$. (b) $j = 5$.

A. Approximation

In high-SNR regime, we can approximate (33) by omitting I_1 and I_2, as f_{SNR} will be between 0 and 1 and $\ln(1+\text{SNR}^{-1})$ will be small as well. Fig. 10 shows that indeed I_1 and the rest R, as defined in (34)–(36) are dominant with respect to I_1 and I_2

for large values of λ_{BS}, the approximation $I_3 + R$ would work well.

We start with the approximation of I_3, as defined in (40). We can express the incomplete gamma function $\Gamma(s,x)$ for $s \in \mathbb{N}$ as [33]:

$$\Gamma(s,x) = \Gamma(s)e^{-x}\sum_{i=0}^{s-1}\frac{x^i}{i!}, \tag{43}$$

which holds for $|x| < 1$, while for large values of x, the incomplete gamma function tends to zero.

For the second term of I_3 in (40), we need to find the approximation of the derivative of the gamma function, which is given in [34]:

$$\begin{aligned}\frac{\mathrm{d}}{\mathrm{d}s}\Gamma(s,x) &= \ln(x)\Gamma(s,x) - x\frac{\mathrm{d}}{\mathrm{d}t}\Gamma(s-t)x^{t-1}\Big|_{t=0} \\ &\quad + \sum_{i=0}^{\infty}\frac{(-1)^i x^{s+i}}{i!(s+i)^2} \\ &= \ln(x)\Gamma(s,x) - \Gamma(s)(\ln(x)+\gamma - H_{s-1}) \\ &\quad + \sum_{i=0}^{\infty}\frac{(-1)^i x^{s+i}}{i!(s+i)^2},\end{aligned} \tag{44}$$

where $H_s = \sum_{i=1}^{s}\frac{1}{i}$ is the harmonic number.

We can now fill in (40) using (43) and (44):

$$\begin{aligned}I_3 &= \frac{\alpha}{2}\Bigg((\ln(\phi) - \ln(\lambda_{BS}\pi))\left(e^{-\lambda_{BS}\pi}\sum_{i=0}^{j-1}\frac{(\lambda_{BS}\pi)^i}{i!} - 1\right) \\ &\quad + \sum_{i=0}^{\infty}\frac{(-1)^i(\lambda_{BS}\pi)^{j+i}}{i!(j+i)^2\Gamma(j)} - \sum_{i=0}^{\infty}\frac{(-1)^i\phi^{j+i}}{i!(j+i)^2\Gamma(j)}\Bigg) \\ &= \ln(c)\left(e^{-\lambda_{BS}\pi}\sum_{i=0}^{j-1}\frac{(\lambda_{BS}\pi)^i}{i!} - 1\right) \\ &\quad + \frac{\alpha}{2\Gamma(j)}\sum_{i=0}^{\infty}\frac{(-1)^i\left((\lambda_{BS}\pi)^{j+i} - \phi^{j+i}\right)}{i!(j+i)^2}.\end{aligned} \tag{45}$$

Assuming $\lambda_{BS}\pi < 1$, we can approximate (45) for $j > 1$:

$$\begin{aligned}I_3 &= \ln(c)\left(e^{-\lambda_{BS}\pi}\left(1+\lambda_{BS}\pi + O\left((\lambda_{BS}\pi)^2\right)\right) - 1\right) \\ &\quad - \frac{\alpha}{2\Gamma(j)}\sum_{i=0}^{\infty}\frac{(-1)^i\phi^{j+i}}{i!(j+i)^2\Gamma(j)}\cdot\left(1+O\left(c^{-\frac{2j}{\alpha}}\right)\right) \\ &= \ln(c)\left(e^{-\lambda_{BS}\pi}\left(1+\lambda_{BS}\pi + O\left((\lambda_{BS}\pi)^2\right)\right) - 1\right) \\ &\quad + \frac{\alpha\phi^j}{2j^2\Gamma(j)}\,{}_2F_2(\{j,j\},\{1+j,1+j\},-\phi)\left(1+O\left(c^{-\frac{2j}{\alpha}}\right)\right),\end{aligned} \tag{46}$$

where ${}_2F_2(a,b,x)$ is the hypergeometric function that we can approximate using Theorem 3.1 of [35]:

$$\begin{aligned}&{}_2F_2(\{j,j\},\{1+j,1+j\},-\phi) \\ &= \frac{(\Gamma(j+1))^2}{(\Gamma(j))^2}\int_0^1 e^{-\phi y}(1-y)y^{j-1}\,{}_2F_1\left(\{1,1\},\{2\},1-y\right)\mathrm{d}y \\ &= \frac{j^2}{\phi^j}\left(\Gamma(j)\left(\ln(\phi)+\gamma - H_{j-1}\right) + G_{2,3}^{3,0}\left(\phi\middle|\begin{matrix}1,1\\0,0,j\end{matrix}\right)\right) \\ &= \frac{j^2\Gamma(j)}{\phi^j}\left(\ln(\phi)+\gamma-H_{j-1}\right) + O\left(j^2\phi^{-2j}\right),\end{aligned} \tag{47}$$

where $G_{2,3}^{3,0}\left(\phi\middle|\begin{matrix}1,1\\0,0,j\end{matrix}\right)$ is the Meijer-G function, which is always smaller than ϕ^{-j} for $\phi > 1$.[2] The approximation in (47) can be substituted in (46) to obtain a final approximation of I_3 for $j > 1$:

$$\begin{aligned}I_3 &= \ln(c)\left(e^{-\lambda_{BS}\pi}\left(1+\lambda_{BS}\pi + O\left((\lambda_{BS}\pi)^2\right)\right) - 1\right) \\ &\quad + \frac{\alpha}{2}(\ln(\phi)+\gamma-H_{j-1})\left(1+O\left(c^{-\frac{2j}{\alpha}}\right)\right) \\ &\quad + O\left(\Gamma(j)^{-1}c^{-\frac{2j}{\alpha}}\phi^{-j}\right).\end{aligned} \tag{48}$$

For $j = 1$, I_3 can directly be calculated from (36):

$$\begin{aligned}I_3 &= \ln(c)e^{-\lambda_{BS}\pi} + \frac{\alpha}{2}\left(\Gamma(0,\phi) - \Gamma(0,\lambda_{BS}\pi)\right) \\ &= \ln(c)e^{-\lambda_{BS}\pi} + \frac{\alpha}{2}\left(-\frac{1}{\phi}e^{-\phi} + \ln(\lambda_{BS}\pi) + \gamma - \lambda_{BS}\pi\right) \\ &\quad + O\left(\phi^{-1}\right) + O\left((\lambda_{BS}\pi)^2\right),\end{aligned} \tag{49}$$

using the series expansion around 0 and around ∞ for $\Gamma(0,x)$.

As $\mathbb{E}(\log_2(1+SNR_j)) = \frac{1}{\ln(2)}(I_1+I_2+I_3)+R$, we still need to approximate I_1, I_2 and R. To approximate R, we again approximate $\Gamma(k,x)$ by the first 2 terms of (43):

$$R = \begin{cases}\log_2(c)\left(1-e^{-\lambda_{BS}\pi}\right) + O\left(c^{-1}\log_2(c)\right), & j=1,\\ \log_2(c)\left(1-e^{-\lambda_{BS}\pi}(1+\lambda_{BS}\pi+O\left((\lambda_{BS}\pi)^2\right)+O\left(c^{-1}\right)\right), & \end{cases} \tag{50}$$

[2] As derived in Wolfram Mathematica.

$$\begin{aligned}\mathbb{E}(\log_2(1+\mathrm{SNR}_j)) &= \frac{1}{\ln(2)\Gamma(j)}G(j,\phi) + \log_2(1+c)\left(1-\frac{\Gamma(j,\lambda_{BS}\pi)}{\Gamma(j+1)}\right) \\ &\quad + \frac{\alpha}{2\ln(2)\Gamma(j)}\left(\ln(\phi)\left(\Gamma(j,\lambda_{BS}\pi)-\Gamma(j,\phi)\right) - \frac{\mathrm{d}}{\mathrm{d}a}\left[\Gamma(a,\lambda_{BS}\pi)-\Gamma(a,\phi)\right]_{a=j}\right)\end{aligned} \tag{41}$$

$$G(j,\phi) = \sum_{i=0}^{\infty}\frac{(-1)^i\phi^{\frac{\alpha}{2}(i+1)}}{i+1}\Gamma\left(\frac{-\alpha}{2}(i+1)+j,\phi\right) + \frac{(-1)^i\phi^{-\frac{\alpha}{2}(i+1)}}{i+1}\left(\Gamma\left(\frac{\alpha}{2}(1+i)+j,\lambda_{BS}\pi\right) - \Gamma\left(\frac{\alpha}{2}(1+i)+j,\phi\right)\right) \tag{42}$$

as the second equation holds for $j > 1$. For I_1 and I_2, we find an upper bound as Fig. 10 shows these integrals are negligible in high-SNR regime:

$$I_1 \leq \ln(2) \cdot \mathbb{P}\left(\text{SNR}_j \leq 1\right) = \ln(2)\frac{\Gamma(j,\phi)}{\Gamma(j)} = O\left(e^{-\phi}\phi^j\right), \tag{51}$$

$$I_2 \leq \ln\left(1 + \frac{1}{\mathbb{E}\left(\text{SNR}_j\right)}\right) = O\left(\mathbb{E}\left(\text{SNR}_j^{-1}\right)\right). \tag{52}$$

Now, we approximate $\mathbb{E}(\log_2(1 + SNR_j))$ by using (49) and (48) together with (50)–(52):

$$\mathbb{E}(\log_2(1 + \text{SNR}_1)) = \frac{\alpha}{2\ln(2)}\left(\ln(\phi) + \gamma - \lambda_{BS}\pi\right) + \delta_1, \tag{53}$$

$$\mathbb{E}(\log_2(1 + \text{SNR}_j)) = \frac{\alpha}{2\ln(2)}\left(\ln(\phi) + \gamma - H_{j-1}\right) + \delta_j, \tag{54}$$

for $j > 1$ and where γ is Euler's constant and for the following variables δ_1 and δ_j:

$$\delta_1 = O\left(\phi^{-1}\right) + O\left((\lambda_{BS}\pi)^2\right) + O\left(\ln(c)c^{-1}\right) + O\left(\mathbb{E}(\text{SNR}_j^{-1})\right),$$

$$\delta_j = O\left(c^{-\frac{2j}{\alpha}}\ln(\phi)\right) + O\left(\Gamma(j)^{-1}c^{-\frac{2j}{\alpha}}\phi^{-j}\right) + O\left(\ln(c)c^{-1}\right) + O\left(\mathbb{E}\left(\text{SNR}_j^{-1}\right)\right),$$

where the latter holds for $j > 1$.

ACKNOWLEDGMENT

We thank A.J.E.M. Janssen for help with the calculations in Appendix A.

REFERENCES

[1] M. Simsek, A. Aijaz, M. Dohler, J. Sachs, and G. Fettweis, "5G-Enabled tactile internet," *IEEE J. Sel. Areas Commun.*, vol. 34, no. 3, pp. 460–473, Mar. 2016.

[2] A. Wolf, P. Schulz, M. Dorpinghaus, J. C. S. Santos Filho, and G. Fettweis, "How reliable and capable is multi-connectivity?," *IEEE Trans. Commun.*, vol. 67, no. 2, pp. 1506–1520, Feb. 2019.

[3] M. T. Suer, C. Thein, H. Tchouankem, and L. Wolf, "Multi-connectivity as an enabler for reliable low latency communications - an overview," *IEEE Commun. Surv. Tut.*, vol. 22, no. 1, pp. 156–169, Jan.–Mar. 2020.

[4] M. Gapeyenko et al., "On the degree of multi-connectivity in 5G millimeter-wave cellular urban deployments," *IEEE Trans. Veh. Technol.*, vol. 68, no. 2, pp. 1973–1978, Feb. 2019.

[5] J. Perdomo, M. Ericsson, M. Nordberg, and K. Andersson, "User performance in a 5G multi-connectivity ultra-dense network city scenario," in *Proc. IEEE 45th Conf. Local Comput. Netw.*, 2020, pp. 195–203.

[6] A. Wolf, P. Schulz, D. Öhmann, M. Dörpinghaus, and G. Fettweis, "Rate-reliability tradeoff for multi-connectivity," in *Proc. IEEE Wireless Commun. Netw. Conf.*, 2018, pp. 1–6.

[7] G. Ghatak, Y. Sharma, K. Zaid, and A. U. Rahman, "Elastic multi-connectivity in 5G networks," *Phys. Commun.*, vol. 43, 2020, Art. no. 101176.

[8] Y. Sharma and G. Ghatak, "A statistical characterization of SINR coverage and network throughput with macro-diversity," in *Proc. IEEE 21st Int. Symp. World Wireless, Mobile Multimedia Netw.*, 2020, pp. 197–204.

[9] D. Moltchanov, A. Ometov, S. Andreev, and Y. Koucheryavy, "Upper bound on capacity of 5G mmWave cellular with multi-connectivity capabilities," *Electron. Lett.*, vol. 54, no. 11, pp. 724–726, 2018.

[10] V. Petrov et al., "Dynamic multi-connectivity performance in ultra-dense urban mmwave deployments," *IEEE J. Sel. Areas Commun.*, vol. 35, no. 9, pp. 2038–2055, Sep. 2017.

[11] M. Gerasimenko, D. Moltchanov, M. Gapeyenko, S. Andreev, and Y. Koucheryavy, "Capacity of multiconnectivity mmWave systems with dynamic blockage and directional antennas," *IEEE Trans. Veh. Technol.*, vol. 68, no. 4, pp. 3534–3549, Apr. 2019.

[12] R. Pirmagomedov, D. Moltchanov, V. Ustinov, M. N. Saqib, and S. Andreev, "Performance of mmwave-based mesh networks in indoor environments with dynamic blockage," in *Proc. Int. Conf. Wired/Wireless Internet Commun.*, 2019, pp. 129–140.

[13] S. Choi, J.-G. Choi, and S. Bahk, "Mobility-aware analysis of millimeter wave communication systems with blockages," *IEEE Trans. Veh. Technol.*, vol. 69, no. 6, pp. 5901–5912, Jun. 2020.

[14] H. ElSawy, A. Sultan-Salem, M. S. Alouini, and M. Z. Win, "Modeling and analysis of cellular networks using stochastic geometry: A tutorial," *IEEE Commun. Surv. Tut.*, vol. 19, no. 1, pp. 167–203, Jan.–Mar. 2017.

[15] B. Błaszczyszyn, M. K. Karray, and H. P. Keeler, "Wireless networks appear Poissonian due to strong shadowing," *IEEE Trans. Wireless Commun.*, vol. 14, no. 8, pp. 4379–4390, Aug. 2015.

[16] J. G. Andrews, F. Baccelli, and R. K. Ganti, "A tractable approach to coverage and rate in cellular networks," *IEEE Trans. Commun.*, vol. 59, no. 11, pp. 3122–3134, Nov. 2011.

[17] B. Blaszczyszyn and M. K. Karray, "Quality of service in wireless cellular networks subject to log-normal shadowing," *IEEE Trans. Commun.*, vol. 61, no. 2, pp. 781–791, Feb. 2013.

[18] Z. Ren, G. Wang, Q. Chen, and H. Li, "Modelling and simulation of rayleigh fading, path loss, and shadowing fading for wireless mobile networks," *Simul. Modelling Pract. Theory*, vol. 19, no. 2, pp. 626–637, 2011.

[19] C. E. Shannon, "A mathematical theory of communication," *ACM SIGMOBILE mobile Comput. Commun. Rev.*, vol. 5, no. 1, pp. 3–55, 2001.

[20] C. Beard and W. Stallings, *Wireless Communication Networks and Systems*. London, U.K.: Pearson, 2015.

[21] T. S. Rappaport et al., *Wireless communications: Principles and practice*. Hoboken, NJ, USA: Prentice Hall – PTR, 2002.

[22] C. Stegehuis and L. Weedage, "Degree distributions in ab random geometric graphs," *Physica A: Stat. Mechanics Appl.*, vol. 586, 2022, Art. no. 126460.

[23] R. Van Der Hofstad, *Random Graphs and Complex Networks: Volume 1*. Cambridge, U.K.:Cambridge Univ. Press, 2016.

[24] R. Irmer et al., "Coordinated multipoint: Concepts, performance, and field trial results," *IEEE Commun. Mag.*, vol. 49, no. 2, pp. 102–111, Feb. 2011.

[25] C. Tatino, I. Malanchini, N. Pappas, and D. Yuan, "Maximum throughput scheduling for multi-connectivity in millimeter-wave networks," in *Proc. IEEE 16th Int. Symp. Model. Optim. Mobile, Ad Hoc, Wireless Netw.*, 2018, pp. 1–6.

[26] M. L. Attiah, A. A. M. Isa, Z. Zakaria, M. Abdulhameed, M. K. Mohsen, and I. Ali, "A survey of mmwave user association mechanisms and spectrum sharing approaches: An overview, open issues and challenges, future research trends," *Wireless Netw.*, vol. 26, no. 4, pp. 2487–2514, 2020.

[27] 3rd Generation Partnership Project (3GPP), "Study on channel model for frequencies from 0.5 to 100 ghz," 3GPP, Sophia Antipolis, France, Tech. Rep. Release 14, 2018.

[28] M. T. Moayyed, F. Restuccia, and S. Basagni, "Comparative performance evaluation of mmwave 5G NR and LTE in a campus scenario," in *Proc. IEEE 92nd Veh. Technol. Conf.*, 2020, pp. 1–5.

[29] R. K. Jain et al., "A quantitative measure of fairness and discrimination," *Eastern Res. Lab., Digit. Equip. Corporation, Hudson, MA, USA*, 1984.

[30] Z. Xiao et al., "A survey on millimeter-wave beamforming enabled UAV communications and networking," *IEEE Commun. Surv. Tut.*, vol. 24, no. 1, pp. 557–610, Jan.–Mar. 2022.

[31] K.-L. Besser, P.-H. Lin, and E. A. Jorswieck, "On fading channel dependency structures with a positive zero-outage capacity," *IEEE Trans. Commun.*, vol. 69, no. 10, pp. 6561–6574, Oct. 2021.

[32] E. Jorswieck and P.-H. Lin, "Ultra-reliable multi-connectivity with negatively dependent fading channels," in *Proc. IEEE 16th Int. Symp. Wireless Commun. Syst.*, 2019, pp. 373–378.

[33] P. Amore, "Asymptotic and exact series representations for the incomplete gamma function," *EPL (Europhys. Lett.)*, vol. 71, no. 1, pp. 1–7, 2005.

[34] K. O. Geddes, M. L. Glasser, R. A. Moore, and T. C. Scott, "Evaluation of classes of definite integrals involving elementary functions via differentiation of special functions," *Applicable Algebra Eng., Commun. Comput.*, vol. 1, no. 2, pp. 149–165, 1990.

[35] H. Volkmer and J. J. Wood, "A note on the asymptotic expansion of generalized hypergeometric functions," *Anal. Appl.*, vol. 12, no. 1, pp. 107–115, 2014.

Lotte Weedage received the M.Sc. degree in applied mathematics from the University of Twente, Enschede, The Netherlands, in 2022. She is currently working toward the Ph.D. degree with the Mathematics Department, University of Twente, where she works on the EERI Project: Energy-Efficient and Resilient Internet. Her research interests include stochastic geometry, mmWave networks, and multi-connectivity.

Clara Stegehuis received the Ph.D. degree from Eindhoven University of Technology, Eindhoven, The Netherlands, in 2019. She is currently an Associate Professor in applied mathematics with the University of Twente, Enschede. Her research interests include stochastic networks and applied probability, with an emphasis on asymptotic analysis, optimization, and randomized algorithms.

Suzan Bayhan received the Ph.D. degree in computer engineering from Bogazici University, Istanbul, Turkey, in 2012. She is currently an Assistant Professor with the University of Twente, Enschede, The Netherlands. Previously, she was with the TU Berlin and the University of Helsinki, Helsinki, Finland. Her research interests include resource management in wireless networks, spectrum sharing, and energy-efficient networking.